Palaeogeography, Palaeoclimatology, Palaeoecology 518 (2019) 10–21

Contents lists available at ScienceDirect

Palaeogeography, Palaeoclimatology, Palaeoecology

journal homepage: www.elsevier.com/locate/palaeo

Spatiotemporal changes in C_4 plant abundance in China since the Last Glacial Maximum and their driving factors

Wenqi Jiang[a,c], Haibin Wu[a,b,c,*], Qin Li[a,d], Yating Lin[a,c], Yanyan Yu[a,b]

[a] Key Laboratory of Cenozoic Geology and Environment, Institute of Geology and Geophysics, Chinese Academy of Sciences, Beijing 100029, China
[b] CAS Center for Excellence in Life and Paleoenvironment, Beijing 100044, China
[c] University of Chinese Academy of Sciences, Beijing 100049, China
[d] CAS Center for Excellence in Tibetan Plateau Earth Sciences, Beijing 100101, China

ARTICLE INFO

Keywords:
Carbon isotopes
Temperature
Atmospheric pCO_2
BIOME4
Holocene

ABSTRACT

Knowledge of changes in the distribution of C_3 and C_4 plants in relation to climate change is the key to predicting the biosphere's response to future climatic warming. There are significant differences in the spatiotemporal evolution of C_4 plant abundance at different latitudes since the Last Glacial Maximum (LGM), and the factors responsible remain debated. In this study, we reconstructed the spatiotemporal pattern of C_4 plants in China since the LGM, based on a synthesis of $\delta^{13}C$ records of soil organic matter from paleosol sequences and $\delta^{13}C$ records of individual n-alkanes from lake and marine sediments. The results indicate that, spatially, maximum C_4 abundance during the LGM was in South China; while maximum C_4 abundance occurred in the Chinese Loess Plateau in North China during the early and mid-Holocene. Temporally, in North China, C_4 plant abundance initially increased since the LGM, reached a maximum during the early and mid-Holocene and then decreased; however, the opposite trend occurred in South China. Combined with a physiological-process model used to study the sensitivity of C_3 and C_4 plants to changes in climate and atmospheric pCO_2 in different regions, our results reveal that temperature was the dominant factor driving C_4 plant expansion in North China, whereas atmospheric pCO_2 and precipitation were the main factors controlling C_4 plant abundance in South China.

1. Introduction

C_3 and C_4 plants use two different pathways for CO_2 fixation. C_3 plants are trees, cold-season grasses and sedges (Sponheimer and Lee-Thorp, 1999), and C_4 plants are warm season grasses and sedges that are mainly distributed in tropical savannas, temperate grasslands and semiarid regions (Sage et al., 1999). The relative abundance of C_3 and C_4 plants depends strongly on atmospheric CO_2 levels (atmospheric pCO_2) and climate. Compared to C_3 plants, C_4 plants have a competitive advantage under low ambient atmospheric pCO_2 and high-water stress (Ehleringer et al., 1997); in addition, C_4 plants are favored by stronger irradiation and higher growing-season temperatures, which enable them to produce more energy during photosynthesis (Samal and Martin, 2013). Thus, ongoing climate change and increasing atmospheric CO_2 concentrations will have a significant impact on the growth of C_3 and C_4 plants.

The global climate system has experienced an overall warming trend from the Last Glacial Maximum (LGM, ~21–18 kyr BP) to the Holocene Thermal Maximum (~10–6 kyr BP), which was followed by a cooling trend (Shakun et al., 2012; Marcott et al., 2013) punctuated by a series of abrupt warming/cooling events (Masson-Delmotte et al., 2013). In addition, atmospheric pCO_2 has increased significantly since the LGM (Lüthi et al., 2008). Therefore, knowledge of the development of C_3 and C_4 plants from the LGM through the Holocene, and their response to climate change, may enable us to anticipate future vegetation trends.

Based on the stable carbon isotopic composition of compound specific and bulk organic matter (Eglinton and Hamilton, 1967; Cerling et al., 1989; Rieley et al., 1991), systematic changes in the relative abundance of C_4 plants since the LGM have been demonstrated in previous studies. At low latitudes, C_4 plants generally decreased from the LGM to the Holocene (Huang et al., 2001; Castañeda et al., 2007; Damsté et al., 2011; Contreras-Rosales et al., 2014; Dubois et al., 2014), while this trend was generally reversed at middle latitudes (Muhs et al., 1999; Johnson and Willey, 2000; Gu et al., 2003; Yang et al., 2015). However, even within a given latitudinal zone, an increasing number of

* Corresponding author at: Key Laboratory of Cenozoic Geology and Environment, Institute of Geology and Geophysics, Chinese Academy of Sciences, Beijing 100029, China.
E-mail address: haibin-wu@mail.iggcas.ac.cn (H. Wu).

https://doi.org/10.1016/j.palaeo.2018.12.021
Received 20 August 2018; Received in revised form 1 December 2018; Accepted 30 December 2018
Available online 03 January 2019
0031-0182/ © 2019 Elsevier B.V. All rights reserved.

records have revealed that C_4 plant abundance varied significantly due to differences in climatic conditions (Rao et al., 2007). Therefore, the reconstruction of C_4 plant abundance at a regional scale needs to be conducted in more detail to fully understand the development of C_4 plants since the LGM.

China, much of which is located in the East Asian monsoon region, has a broad range of climatic conditions and provides an excellent location to evaluate the interactions between climate and vegetation. Previous studies suggested that on the Chinese Loess Plateau (CLP) C_4 plants generally increased in abundance from the LGM to the Holocene (e.g., Gu et al., 2003; Liu et al., 2005; Yang et al., 2015); while in contrast, in South China, C_4 plant abundance decreased from the LGM to the Holocene (e.g., Zhou et al., 2012; Kuang et al., 2013; Yang et al., 2015). However, previous analyses focused mainly on vegetation changes at individual sites, and spatial patterns of vegetation have received much less attention. Thus, a synthesis of paleovegetation data is needed to determine the spatiotemporal pattern of C_4 abundance for the whole of China, which would potentially enable the driving mechanisms to be determined. Increased C_4 abundance on the CLP during the Holocene was interpreted to be caused by increasing temperature (Gu et al., 2003; Zhang et al., 2003) or increasing East Asian monsoon intensity (Vidic and Montañez, 2004; Liu et al., 2005; Yang et al., 2015); while the decreased C_4 abundance in South China was interpreted as a response to increased monsoon precipitation during the Holocene (Xue et al., 2014; Zhang et al., 2017). Thus, the causes of C_4 plant expansion in different regions require further study.

These contrasting views regarding the principal driver of C_4 plant abundance may result either from uncertainties in the interpretation of the climatic proxies (Wang, 2009; Chen et al., 2016), or from the fact that previous studies failed to distinguish the effects of temperature, precipitation and atmospheric CO_2 concentration on C_4 plant growth (Wu et al., 2014). Therefore, to distinguish the relative importance of these factors and to establish the cause of changes in C_4 plant abundance in different regions, it is important to develop a new approach to the study the sensitivity of C_3 and C_4 plants to temperature, precipitation and atmospheric pCO_2.

In this study, we reconstructed the spatiotemporal pattern of development of C_4 plants across China since the LGM based on a synthesis of $\delta^{13}C$ values of soil organic matter (SOM) from paleosol sequences, and records of individual n-alkanes from lake and marine sediments. Subsequently, we used BIOME4 (Kaplan et al., 2003; Hatté and Guiot, 2005), a vegetation model which incorporates the physiological responses of C_3 and C_4 plants to changes in atmospheric pCO_2, temperature and precipitation, to investigate how well changes in atmospheric pCO_2 and climate parameters explain the observed distribution of C_3 and C_4 plants in various regions in China since the LGM.

2. Data and methods

China is located in the East Asian landmass, where the East Asian monsoon plays an important role in driving hydrological and energy cycles (Chen et al., 1991). Precipitation is concentrated in the warmer months, and the annual total ranges from < 200 mm in the northwest to ~2000 mm in the southeast (Fig. S1a). The mean annual temperature ranges from < 0 °C in the northeast to 20 °C in the southeast (Fig. S1b). The geographical extent and complex topography contribute to produce an extremely diverse climate in China, which varies from tropical in the south, subarctic in the north, and alpine in the higher elevation region of the Tibetan Plateau. The vegetation follows the southeast-northwest precipitation gradient, changing from a moist coastal forest zone to desert in the northwest, with steppe in the middle. In the East Asian monsoon area, forest composition changes with the temperature gradient, from tropical rainforest in the south to boreal coniferous forest in the north (Hou, 2001). An investigation of the distribution of C_4 plants indicated that 90% of C_4 species consist of Poaceae, Cyperaceae, and Chenopodiceae, and that in general, the total number of C_4 species decreases from south to north and from east to west (Yin and Li, 1997; Wang and Ma, 2016).

2.1. Data selection

Because of the changes in carbon isotopic composition caused by physiological differences during CO_2 uptake during photosynthesis, C_3 plants have $\delta^{13}C$ values ranging from −22‰ to −30‰, whereas C_4 plants have values ranging from −10‰ to −14‰ (Bender, 1971; Farquhar, 1983). $\delta^{13}C$ records from loess-paleosol sequences and lacustrine and marine sediments have been used to document past changes in the abundances of C_3 and C_4 plants, and a synthesis of these records provides a useful means of reconstructing the spatiotemporal representation of C_4 plants across China.

In general, the $\delta^{13}C$ of buried SOM in loess-paleosol sequences reflects the $\delta^{13}C$ composition of the organic matter derived from the parent vegetation, with little or no isotopic fractionation (Melillo et al., 1989; Wang et al., 2008); thus, it is a well-established means of reconstructing the relative abundance of C_3 and C_4 plants (Cerling et al., 1989). For lake and marine sediments, the carbon isotopic values of long-chain leaf waxes n-alkanes (n-C_{27}, n-C_{29}, or n-C_{31}), which originate primarily from terrestrial higher plants (Rieley et al., 1991; Eglinton and Hamilton, 1967), provide more specific information on past changes in C_3 and C_4 plant abundance on land than is provided by bulk organic matter, since the latter includes input from both terrestrial and aquatic sources (Huang et al., 1999, 2001).

In this study, we compiled and synthesized $\delta^{13}C$ records from the literature. $\delta^{13}C$ records were selected based on the following four criteria: (1) Records should be $\delta^{13}C$ values of SOM from loess-paleosol deposits, or $\delta^{13}C$ values of higher plant-derived long-chain n-alkanes (n-C_{27}, n-C_{29}, or n-C_{31}) from lacustrine and marine deposits. (2) Records should span at least 5 kyr. (3) A reliable chronology was available. In addition, for each paleosol sequence, a magnetic susceptibility record was available for the same section, enabling high-resolution stratigraphic correlation (Heller and Liu, 1984). For lake and marine sediments, a minimum of three independent age control points, e.g., accelerator mass spectrometry radiocarbon dating (AMS ^{14}C) and liquid scintillation counting radiocarbon dating (LSC ^{14}C), should be available for each record. (4) The sampling resolution was better than 2000 years.

Based on these criteria, 33 $\delta^{13}C$ records of SOM from loess-paleosol sequences and 16 $\delta^{13}C$ records of long-chain n-alkanes from lake and marine sediments were considered suitable for the study. All $\delta^{13}C$ records are derived from previous publications, except $\delta^{13}C$ record of SOM for Zhouzhuang loess-paleosol section which is generated by ourselves (see Table S1 for detailed information for selected sites and Text S1 for sampling and experimental methods of Zhouzhuang section). In addition, published $\delta^{13}C$ values of modern surface soils (N = 1050) and modern plants (N = 1872) in China were assembled (see Table S2 for detailed site information). To facilitate assessment of the spatiotemporal distribution of C_4 plants, four sub-regions were defined for China based on physical geographic regionalization (Luo, 1954): Northeast China, the CLP, South China and the Tibetan Plateau (Fig. 1).

2.2. Chronology

The age control for the lake and marine sediment sequences is based mainly on ^{14}C ages determined by accelerator mass spectrometry (AMS) (98.8% AMS ^{14}C, 1.2% LSC ^{14}C). To obtain comparable chronologies for all records, we performed a calibration procedure prior to establishing the age model for each site. At individual sites, all radiocarbon ages were first corrected, if reservoir effects are described in the original publication, to remove any old-carbon effects using information provided in the original papers. The corrected ^{14}C ages were then calibrated using the Intcal13 calibration dataset (Reimer et al., 2013). Age-

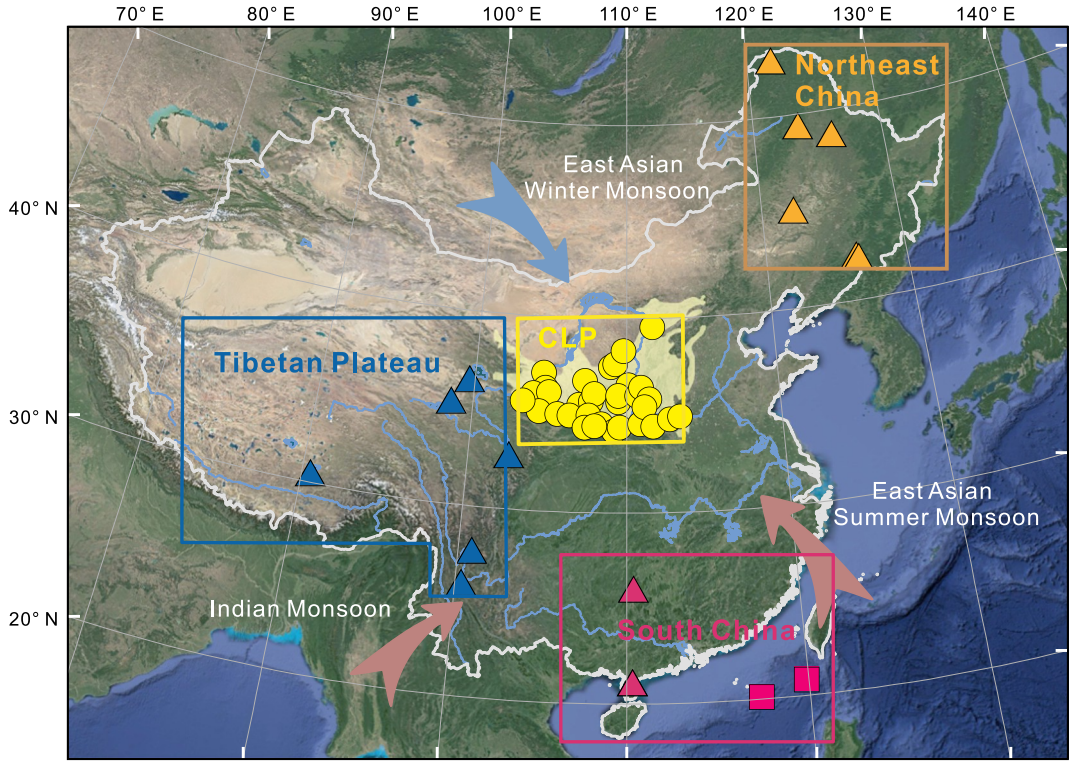

Fig. 1. The study region, sub-regions, trajectories of modern monsoonal circulation and location of study sites.
Triangles: lake records; squares: marine records; circles: loess-paleosol sequences. The yellow shading represents the CLP. Arrows indicate the direction of the winter and summer monsoonal winds. Orange triangles, yellow circles, red triangles and squares, and blue triangles, are in Northeast China, the CLP, South China, and the Tibetan Plateau, respectively. (For interpretation of the references to color in this figure legend, the reader is referred to the web version of this article.)

depth models were then determined using linear interpolation between adjacent calibrated ages.

The loess-paleosol sequences of the CLP are readily correlated, especially from their magnetic susceptibility records which can be matched in detail from site-to-site across the plateau, and which provide a high-resolution stratigraphic tool (Heller and Liu, 1984). We correlated the magnetic susceptibility record of the Weinan-1 section (Kang et al., 2013), for which a high resolution OSL chronology was available, with the magnetic susceptibility records of the other sites. This enabled seven age control points to be applied to all the stable carbon isotope records used in the study (Fig. S2). The ages of the sediment depths between the age control points were then estimated by interpolation using a magnetic susceptibility model (Kukla and An, 1989).

2.3. Reconstruction of C_3 and C_4 plant abundance

Changes in environmental factors, such as precipitation, temperature, $\delta^{13}C$ of atmospheric CO_2 ($\delta^{13}C_{atm}$) and atmospheric CO_2 concentration, can affect the $\delta^{13}C$ values of C_3 and C_4 plants (Farquhar et al., 1989; Brugnoli and Farquhar, 2000). Thus, consideration of these factors is very important for reconstructing variations in C_3 and C_4 plant abundance. However, here, we only consider the effect of changes in $\delta^{13}C_{atm}$ and ignore the effects of changes in climate (precipitation and temperature) and atmospheric CO_2 concentration. The reasons for this are as follows: First, a strong positive relationship between temperature and precipitation exists in the East Asian monsoon region, which is characterized by fluctuations in warm/wet and cool/dry conditions (Liu, 1985; Chen et al., 1991). Although coefficients of −0.40‰/100 mm and 0.104‰/°C have been reported for C_3 plants with respect to changes in precipitation and temperature (Wang et al., 2008, 2013), the precipitation and temperature factors would cancel each other out. Thus, the combined effect of changing climate on the $\delta^{13}C$ of C_3 plants is likely to be insignificant; for example, the combined effect is ~−0.3‰ to 0.5‰ for the LGM and ~−0.3‰ to −0.1‰ for the mid-Holocene on the CLP, representing two climatic extremes (see Table 2 for climate anomalies which are expressed as deviations from the present). No significant coefficients were found for C_4 plants (Wang et al., 2008, 2013). Second, although plants may exhibit short-term phenotypic and isotopic changes in response to abrupt changes in atmospheric pCO_2 (Schubert and Jahren, 2012), they tend to evolve towards an optimal physiology whose isotopic fractionation is pCO_2-independent on geological timescales (Diefendorf et al., 2015; Voelker et al., 2016; Kohn, 2016). Thus, the effects of variations in atmospheric pCO_2 on the $\delta^{13}C$ values of plants since the LGM are likely to be insignificant.

To estimate the $\delta^{13}C$ of modern C_3 and C_4 plants, we calculated the median $\delta^{13}C$ values of C_3 and C_4 plants, respectively, based on the collected $\delta^{13}C$ values of modern plants (N = 1872). High elevation areas are the terrestrial habitats where climate, atmospheric pressure and solar radiation differ substantially from 'normal' levels at low elevations (Körner et al., 1988). The combined effects of these environmental factors lower the ratio between intercellular and atmospheric concentration of CO_2 (*Ci/Ca*) (Farquhar et al., 1989), and the foliar $\delta^{13}C$ values from plants obtained from high elevation sites are therefore significantly higher than those from lower elevations (Körner et al., 1988; Van de Water et al., 2002; Körner, 2007; Zhu et al., 2010; Zhou et al., 2011). In this study, the median $\delta^{13}C$ values of modern C_3 and C_4 plants were calculated for two regions: the Tibetan Plateau (i.e. high elevations) and the other regions of China, at much lower elevations (Table 1). After correcting for the effect of $\delta^{13}C_{atm}$ and for soil organic matter degradation, we assigned respective $\delta^{13}C$ end-member values for C_3 and C_4 plants of −23.8‰ and −9.9‰ for the Tibetan Plateau, and −25.1‰ and −10.6‰ for the rest of China (Table 1).

For the $\delta^{13}C$ records of loess-paleosol sequences, C_4 plant percentages were estimated using the following isotope mass-balance equation (Balesdent and Mariotti, 1996):

Table 1
End-member $\delta^{13}C$ values for C_3 ($\delta^{13}C_{C3}$) and C_4 plants ($\delta^{13}C_{C4}$).

Factors	$\delta^{13}C_{C3}$ (‰)	$\delta^{13}C_{C4}$ (‰)	References
China excluding the Tibetan Plateau			
Modern vegetation	−27.6	−13.1	See Table S2 for site information
$\delta^{13}C_{atm}$ correction (+1.5‰)[a]	−26.1	−11.6	Mauna Loa Observatory, 2000; Schmitt et al., 2012
Degradation correction (+1.0‰)	−25.1	−10.6	Melillo et al., 1989
Tibetan Plateau			
Modern vegetation	−26.3	−12.4	See Table S2 for site information
$\delta^{13}C_{atm}$ correction (+1.5‰)[a]	−24.8	−10.9	Mauna Loa Observatory, 2000; Schmitt et al., 2012
Degradation correction (+1.0‰)	−23.8	−9.9	Melillo et al., 1989

[a] Antarctic ice cores show that $\delta^{13}C_{atm}$ ranged from −6.7‰ to −6.3‰ during the past 21 kyr BP, with an average $\delta^{13}C_{atm}$ of −6.5‰ (Schmitt et al., 2012). The $\delta^{13}C_{atm}$ for the present-day increases to −8.0‰ (Mauna Loa Observatory, 2000), which may be largely explained by the incorporation of atmospheric CO_2 that is depleted in ^{13}C from fossil fuel combustion, and by changes in isotopic fractionation during air/sea gas exchange (Freyer and Belacy, 1983; Schmitt et al., 2012). Here, we assume this 1.5‰ excursion for $\delta^{13}C_{atm}$ correction.

$$C_4(\%) = (\delta^{13}C_{SOM} - \delta^{13}C_{C3})/(\delta^{13}C_{C4} - \delta^{13}C_{C3}) \times 100 \quad (1)$$

where $\delta^{13}C_{C3}$, $\delta^{13}C_{C4}$ are the end-member $\delta^{13}C$ values of C_3 and C_4 vegetation; $\delta^{13}C_{SOM}$ is the $\delta^{13}C$ of SOM; and C_4 (%) is the percentage of C_4 plants in the local vegetation. For the $\delta^{13}C$ records from lake sediments, weighted mean $\delta^{13}C$ values of the n-$C_{27–31}$ alkanes (hereafter referred to as $\delta^{13}C_{27–31}$) were obtained (Collister et al., 1994) using the following equation:

$$\delta^{13}C_{27-31} = (\delta^{13}C_{27} \times C_{27} + \delta^{13}C_{29} \times C_{29} + \delta^{13}C_{31} \times C_{31}) /(C_{27} + C_{29} + C_{31}) \quad (2)$$

where C_{27}, C_{29} and C_{31} are the respective relative abundances of n-C_{27}, n-C_{29} and n-C_{31}, and $\delta^{13}C_{27}$, $\delta^{13}C_{29}$, $\delta^{13}C_{31}$ represent the respective $\delta^{13}C$ values of n-C_{27}, n-C_{29}, n-C_{31}.

To compare C_4 plant percentages calculated using long-chain n-alkanes $\delta^{13}C$ values with those obtained from SOM $\delta^{13}C$ values, it is necessary to correct the range of $\delta^{13}C_{27–31}$ values to make them consistent with the values of $\delta^{13}C_{SOM}$. Previous studies found that $\delta^{13}C_{27–31}$ was depleted by 6–12‰ relative to $\delta^{13}C_{SOM}$, with an average of 8.1‰, which does not change with increasing latitude (Rao et al., 2008). In this study, we use this 8.1‰ difference to correct the $\delta^{13}C_{27–31}$ values. Then, the corrected $\delta^{13}C_{27–31}$ was applied to the isotope mass-balance equation to estimate C_4 abundance, in the same way as for $\delta^{13}C_{SOM}$.

To reconstruct a spatiotemporal pattern of C_4 abundance for each 1000-year time interval since the LGM, we resampled each of the original time series at a 1000-year interval by averaging the original data in each time window (e.g., the value for 1 kyr BP was the average during 0.5 to 1.5 kyr BP, and so on). The spatial distribution of C_4 abundance was illustrated using ArcGIS. Temporal changes in C_4 abundance during the last 21 kyr BP in the four sub-regions (including Northeast China, the CLP, South China and the Tibetan Plateau) were constructed by averaging the estimated C_4 abundance in the respective regions.

2.4. Sensitivity analysis of the effects of climate and atmospheric pCO_2 on C_3/C_4 plants

A novel aspect of this study is the application of a physiological process-based vegetation model, BIOME4 (Kaplan et al., 2003; Hatté and Guiot, 2005), to study the sensitivity of C_3 and C_4 plants to changes in climate and atmospheric pCO_2 since the LGM. The discrimination model to calculate isotopic fractionation during photosynthesis produced by C_3 and C_4 plants is conceptually related to the model of Lloyd and Farquhar (1994). The maximum potential *Ci/Ca* ratio is prescribed for each PFT and the actual *Ci/Ca* is subsequently calculated though iterative optimization. The mean annual isotopic fractionation is calculated by weighting monthly fractionation by the respective NPP. Finally, all the isotopic fractions of both C_3 and C_4 photosynthetic pathways for all coexisting PFTs are considered and weighted by NPP (Hatté and Guiot, 2005).

The model was fed with input consisting of monthly climatic variables (temperature and precipitation), atmospheric pCO_2, and data on soil textural class. The modern atmospheric CO_2 concentration was set to 380 ppmv because most of the modern plants and surface soil samples were collected during 2000s. Soil properties were derived from the FAO digital soil map of the world (Food and Agriculture Organization (FAO), 1995). The modern monthly climatic variables were spatially interpolated from the dataset compiled by the Chinese Central Meteorological Office. We used the artificial neural network technique as described by (Guiot et al., 1996) for interpolation. The BIOME4 model was run at a spatial resolution of 0.5° × 0.5°.

To identify the dominant factor linking climate and atmospheric pCO_2 with the observed changes in C_4 plant abundance, the range of input parameters used for the BIOME4 model should cover their respective ranges of variation since the LGM. Studies have demonstrated that the climatic conditions during the LGM were significantly colder and drier than at present (Jiang et al., 2011; Bartlein et al., 2011); in addition, the early-to-mid Holocene was the warmest and wettest period of the entire post-LGM interval (Shi et al., 1993; Wu et al., 2017). Therefore, the ranges of the climate parameters used for sensitivity experiments are set according to the reconstructed temperature and precipitation during these two periods (Table 2). In addition, atmospheric pCO_2 was increased from the LGM level of ~180 ppmv to ~380 ppmv (Lüthi et al., 2008; Mauna Loa Observatory; Table 2).

Based on the estimated temperature, precipitation and CO_2 concentration, we performed three sensitivity experiments, using the single variable method, for Northeast China, the CLP, South China and the Tibetan Plateau (Table 2). The following model parameters were used:

Table 2
Ranges of the parameters used for sensitivity experiments in the four sub-regions of China since the LGM.

Sub-region	ΔT range (°C)[a]	ΔP range (%)[b]	CO_2 concentration (ppmv)
Northeast China	[−7, +4]	[−20, +50]	[180, 380]
CLP	[−7, +4]	[−50, +30]	
South China	[−3, +2]	[−10, +50]	
Tibetan Plateau	[−4, +5]	[−50, +50]	

The climate ranges are given in terms of the deviation from modern values (°C for temperature and % for precipitation). T, mean annual temperature; P, mean annual precipitation.

[a] In Northeast China, CLP, South China and Tibetan Plateau, palaeotemperature reconstructions have revealed that during the early and mid-Holocene the mean annual temperature (MAT) was higher than today by ~4 °C (Wu et al., 2017), ~4 °C (Shi et al., 1993), ~2 °C (Wu et al., 2017) and ~5 °C (Shi et al., 1993) in the four sub-regions, respectively; while at the LGM, the MAT was lower than today by ~7 °C (Liu, 1988), ~7 °C (Peterse et al., 2011), ~3 °C (Wang et al., 2012), and ~4 °C (Herzschuh et al., 2014) in the four sub-region, respectively.

[b] In Northeast China, CLP, South China and Tibetan Plateau, palaeoprecipitation reconstructions have revealed that during the mid-Holocene, the mean annual precipitation (MAP) was greater than today by ~230 mm (a difference of ~50%) (Wu et al., 2017), ~130 mm (a difference of ~30%) (Chen et al., 2015), ~480 mm (a difference of ~50%) (Wu et al., 2017), and ~200 mm (a difference of ~50%) (Wu et al., 2017) in the four sub-regions, respectively; in contrast, at the LGM, MAP was lower than today by ~70 mm (a difference of ~20%) (Wu et al., 2018), ~100–300 mm (a difference of ~20–50%) (Wu et al., 2002), ~100 mm (a difference of ~10%) (Wu et al., 2018) and ~390 mm (a difference of ~50%) (Herzschuh et al., 2014), respectively.

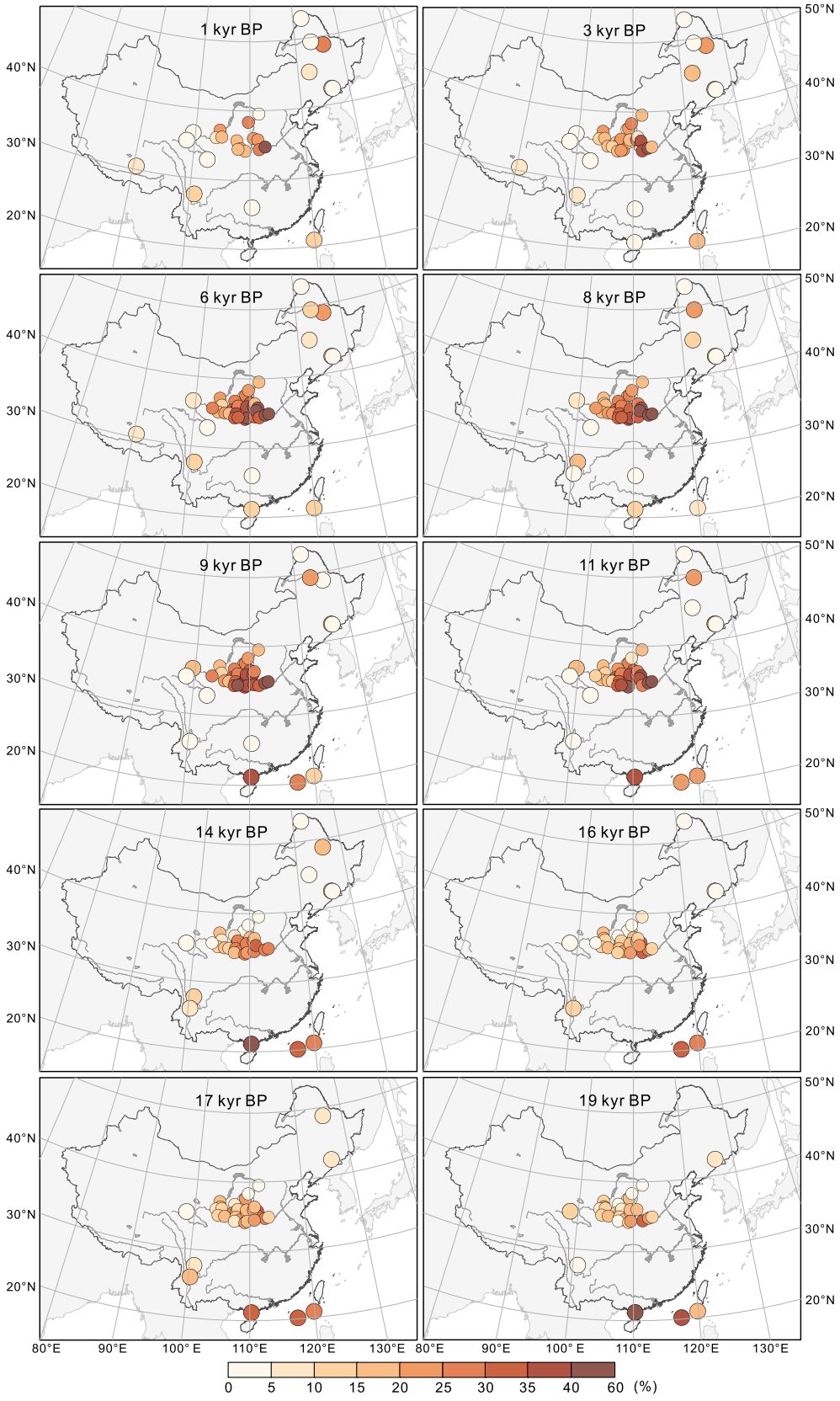

Fig. 2. Spatiotemporal distribution of C_4 plant abundance in China since the LGM.

(1) When temperature was increased from the LGM level to the early-mid Holocene level, precipitation and CO_2 were kept at modern values. (2) When precipitation was increased from the LGM level to the early-mid Holocene level, temperature and CO_2 were kept at modern values. (3) When the CO_2 concentration was increased from 180 ppmv to 380 ppmv, temperature and precipitation were kept at modern values.

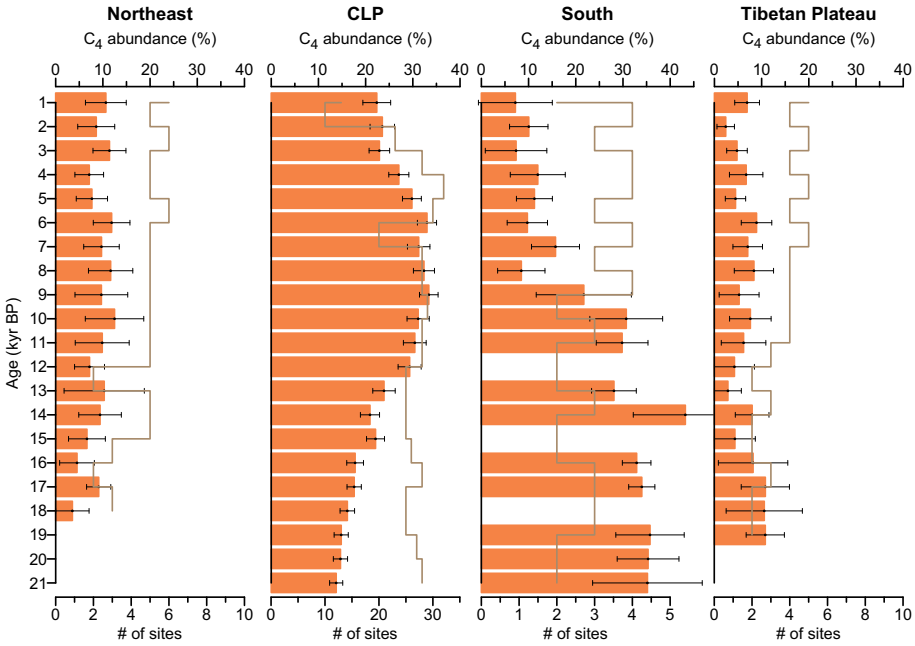

Fig. 3. Temporal changes in C_4 plant abundance of the four sub-regions of China since the LGM. The values are means, and the error bars represent the standard error of the mean. Step-wise lines indicate number of records for each region.

3. Results

3.1. Spatiotemporal distribution of C_4 plant abundance since the LGM

The spatiotemporal distribution of C_3 and C_4 plants is shown in Fig. 2 and Fig. S4. During 21–16 kyr BP, South China had the highest C_4 abundance (as much as 30–45%); from 16 to 9 kyr BP, C_4 abundance increased significantly on the CLP in northern China, with the highest abundance (up to ~40–60%) during 9–6 kyr BP; and thereafter, there was a general decrease in C_4 plant representation throughout China. In addition, for most of the past 21 kyr, C_4 plants on the Tibetan Plateau were less abundant (< 10%) compared to other regions in China, such as South China and the CLP.

3.2. Temporal variation of C_4 abundance within the four sub-regions since the LGM

The temporal variation of C_4 plants in the four sub-regions is shown in Fig. 3. In Northeast China, C_4 abundance generally increased since the LGM (21–19 kyr BP), reached a maximum (up to ~12%) during 10–6 kyr BP. A similar pattern occurred on the CLP, but the amplitude of changes in C_4 abundance was much greater than in Northeast China. Specifically, C_4 abundance remained relatively stable at ~14% from 21 to 19 kyr BP and then increased significantly (by up to ~20%) from 16 to 10 kyr BP, reaching a maximum of ~32% during 10–6 kyr BP. Subsequently, C_4 abundance gradually decreased to ~22% at the present-day. By contrast, South China exhibits the opposite trend: C_4 representation was as high as ~35–43% during 21–10 kyr BP and was ~10% after 9 kyr BP. In the case of the Tibetan Plateau, the abundance C_4 plants remained roughly constant (< 10%) during the past 21 kyr.

3.3. Impact of climate change and atmospheric pCO_2 on the relative abundance of C_4 plants

The BIOME4 model has successfully simulated the discrimination of carbon isotopes in the leaves of C_3 and C_4 plants (Hatté and Guiot, 2005) in Australia (Stewart et al., 1995) and in the southeastern United States (Van de Water et al., 2002). However, for the present study, it is necessary to evaluate the reliability of the BIOME4 model for China. Validation was implemented using the modern carbon isotope dataset collected for China (including 1050 surface soils and 1872 plants - see Table S2 for detailed information). Since the carbon isotopic composition of different types of plant at the same site is quite different, each $\delta^{13}C$ value was classified into one of the 14 vegetation types specified in BIOME4 to determine the isotopic differences between different regions and different vegetation types. Linear regression analysis was used to compare the simulated $\delta^{13}C$ values at each site compared with the observed values. The correlation coefficient (R^2) is 0.90 ($y = 0.88x - 1.95$) between simulated (y) and measured $\delta^{13}C$ (x), indicating that the isotope model of BIOME4 is effective at simulating the carbon isotope discrimination of C_3 and C_4 plants in China (Fig. 4).

The results of sensitivity experiments to evaluate the response of C_4 abundance to changes in temperature, precipitation and atmospheric pCO_2 in the four sub-regions are shown in Fig. 5. Similar results were obtained for both Northeast China and the CLP (Fig. 5a, b): C_4 abundance responded positively to increased temperature, especially within the high temperature range, suggesting that C_4 plants were favored by higher temperatures. In contrast, C_4 abundance responded negatively to increases in atmospheric pCO_2 and precipitation, indicating that C_4 plants are favored by less precipitation and/or lower CO_2 levels. In addition, C_4 plants responded more rapidly to temperature than to atmospheric pCO_2 and precipitation. In South China, C_4 abundance was also positively correlated to temperature and negatively correlated to precipitation and CO_2 concentrations (Fig. 5c). However, the increase in C_4 abundance in response to temperature was much weaker for Northeast China and the CLP.

For the Tibetan Plateau, C_4 abundance was insensitive to changes in temperature, precipitation and atmospheric pCO_2 (Fig. 5d). Almost no change in C_4 abundance is observed when temperature, precipitation and CO_2 concentration were increased since the LGM.

4. Discussion

4.1. Comparison of the results with published records of C_4 plant abundance

Changes in the abundance of C_3 and C_4 plants within vegetation has also been documented by other proxies, including compound-specific carbon isotope records of long-chain n-alkanes from loess-paleosol

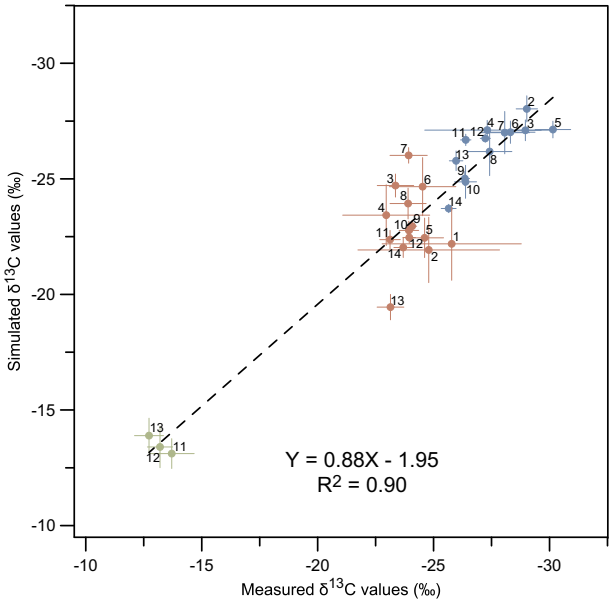

Fig. 4. Results of regression analysis of simulated and measured $\delta^{13}C$ values. The blue dots represent modern C_3 plants samples, green dots represent modern C_4 plants samples, and the red dots represent surface soil samples. Error bars represent 95% confidence intervals. The number indicates the vegetation types: 1, tropical evergreen broadleaf forest; 2, tropical semi-deciduous forest; 3, temperate deciduous forest; 4, temperature conifer forest; 5, warm mixed forest; 6, cool mixed forest; 7, cool confiner forest; 8, cold mixed forest; 9, evergreen taiga/montane forest; 10, deciduous taiga/montane forest; 11, temperate xerophytic shrubland; 12, temperate grassland; 13, desert; 14, tundra. The dataset of $\delta^{13}C$ values consists of measurements of 1050 samples of modern plants and 1872 surface soil samples from across China. (For interpretation of the references to color in this figure legend, the reader is referred to the web version of this article.)

sequences ($\delta^{13}C_{n\text{-alkanes}}$) (Collister et al., 1994; Tipple and Pagani, 2010), the carbon isotopic composition of black carbon from lake sediments ($\delta^{13}C_{BC}$) (Clark et al., 2001), and carbonate $\delta^{13}C$ values of cave stalagmites ($\delta^{13}C_{carb}$) (Dorale et al., 1992, 1998). It is noteworthy that records of $\delta^{13}C_{n\text{-alkanes}}$ from the Xifeng, Luochuan and Xunyi loess-paleosol sequences (Fig. 6a, Zhang et al., 2003; Liu et al., 2005) consistently indicate that C_4 abundance on the CLP generally increased from the LGM to early Holocene and then subsequently decreased. This finding is generally consistent with our reconstruction of C_4 abundance on the CLP (Fig. 6b). In addition, $\delta^{13}C_{BC}$ records from Lake Tengchongqinghai (TCQH), Lake Erhai (Fig. 6c, Zhang et al., 2015, 2017), and $\delta^{13}C_{carb}$ records from Xiangshuiyan and Dongge caves (Fig. 6d, Qin et al., 2000; Zhang et al., 2004) consistently reveal that C_4 plants in South China were less abundant during the LGM compared to the Holocene, which also agree with our result in South China (Fig. 6e).

Nevertheless, despite the trends being broadly similar between the reconstructed C_4 abundance in this study and the additional sites, there are some discrepancies: for example, the timing of highest $\delta^{13}C$ values in Luochuan site slightly leaded (by 2 ka) our result (Fig. 6a, b); $\delta^{13}C_{BC}$ record form Lake TCQH exhibited an increasing trend since 8 kyr BP (Fig. 6c), but there was no significant change in the corresponding C_4 abundance in South China (Fig. 6e); the C_4 abundance peaked during the last 1.5 kyr BP at Xiangshuiyan Cave (Fig. 6d), but the corresponding C_4 abundance was low in South China (Fig. 6e). These subtle differences may be attributed to the fact that the synthesized C_4 abundance in this study indicates regional changes in vegetation, whereas the selected records reflect vegetation change at an individual site.

Although previous studies have investigated temporal changes in the relative abundance of C_3 and C_4 plants at individual sites in China since the LGM, spatial patterns have rarely been addressed. Moreover, previous investigations focused mainly on the spatial pattern of C_4 plant representation on the CLP during key intervals (e.g. the LGM and the mid-Holocene) (Yao et al., 2011; Yang et al., 2015), but the evolution of the spatial pattern of C_4 plant representation at a national scale since the LGM is unclear. Our study represents a significant advance over previous studies in that our data represent most of China, and thus it provides a more comprehensive picture of the spatiotemporal evolution of C_4 plants since the LGM.

The temporal pattern of $\delta^{13}C$ records from Northeast China and the CLP are consistent with records of the $\delta^{13}C$ of the SOM content of aeolian deposits in the Central Great Plains of North America (e.g., Muhs et al., 1999; Johnson and Willey, 2000), and with records of the $\delta^{13}C$ composition of long-chain n-alkanes from the sediments of the North Pacific Ocean and Japan Sea (e.g., Yamada and Ishiwatari, 1999; Ratnayake et al., 2006). These records reveal a shift from a predominantly C_3 community to a mixture of C_3 and C_4 plants at mid-latitude regions from the LGM to the Holocene. At low latitudes, the temporal pattern of our results for South China are also in agreement with $\delta^{13}C$ values of long-chain n-alkanes from tropical Africa (Castañeda et al., 2007; Berke et al., 2012; Wang et al., 2013; Norström et al., 2014), Mesoamerica (e.g., Huang et al., 2001, 2006) and the Bay of Bengal (e.g., Galy et al., 2008; Contreras-Rosales et al., 2014), where higher proportions of C_4 vegetation are evident during the LGM than during the Holocene.

However, due to the limited number of $\delta^{13}C$ records of individual n-alkanes from lake and marine sediments, there are still some degree of uncertainty regarding the reconstructed spatiotemporal evolution of C_4 plant abundance in Northeast China, South China and Tibetan Plateau. These regions require more investigation in the future.

4.2. Possible causes of the patterns of C_4 plant expansion in different regions of China

Two main mechanisms have been invoked to explain changes in the proportion of C_4 plants during glacial-interglacial cycles in China. First, variation in summer monsoon intensity have been proposed as a major factor (Vidic and Montañez, 2004; Liu et al., 2005; Xue et al., 2014; Zhang et al., 2017), based on observations that proxies of summer monsoon intensity (e.g. magnetic susceptibility of loess deposits and $\delta^{18}O$ values of stalagmites) co-vary significantly with the relative abundance of C_4 plants. Second, temperature has been proposed as the main driver of the relative abundance of C_3 and C_4 plants (Gu et al., 2003; Zhang et al., 2003; Rao et al., 2012; Wang et al., 2015), based on the observation that the increasing temperatures from the LGM to Holocene were accompanied by an increase in the representation of C_4 plants.

In the present study, a physiological process-based model was used to distinguish the effects of temperature, precipitation and atmospheric pCO_2 on C_4 plants in different regions of China. In addition, we compared the temporal variation of reconstructed percentages of C_4 plants with records of climate change and CO_2 concentration (Fig. 7), to further determine the dominant factor affecting the evolution of C_4 plants for different regions since the LGM.

Sensitivity analysis indicated that C_4 plants have a competitive advantage over C_3 plants under conditions of low atmospheric CO_2 content and aridity on the CLP (Fig. 5b), because of their ability to concentrate CO_2 and their greater water-use efficiency (Collatz et al., 1998; Raven et al., 1999; Sage, 2001). However, comparison of the record of C_4 abundance with reconstructed precipitation and atmospheric pCO_2 since the LGM (Fig. 7a, c), reveals that an increased abundance of C_4 plants occurred at times of higher precipitation and

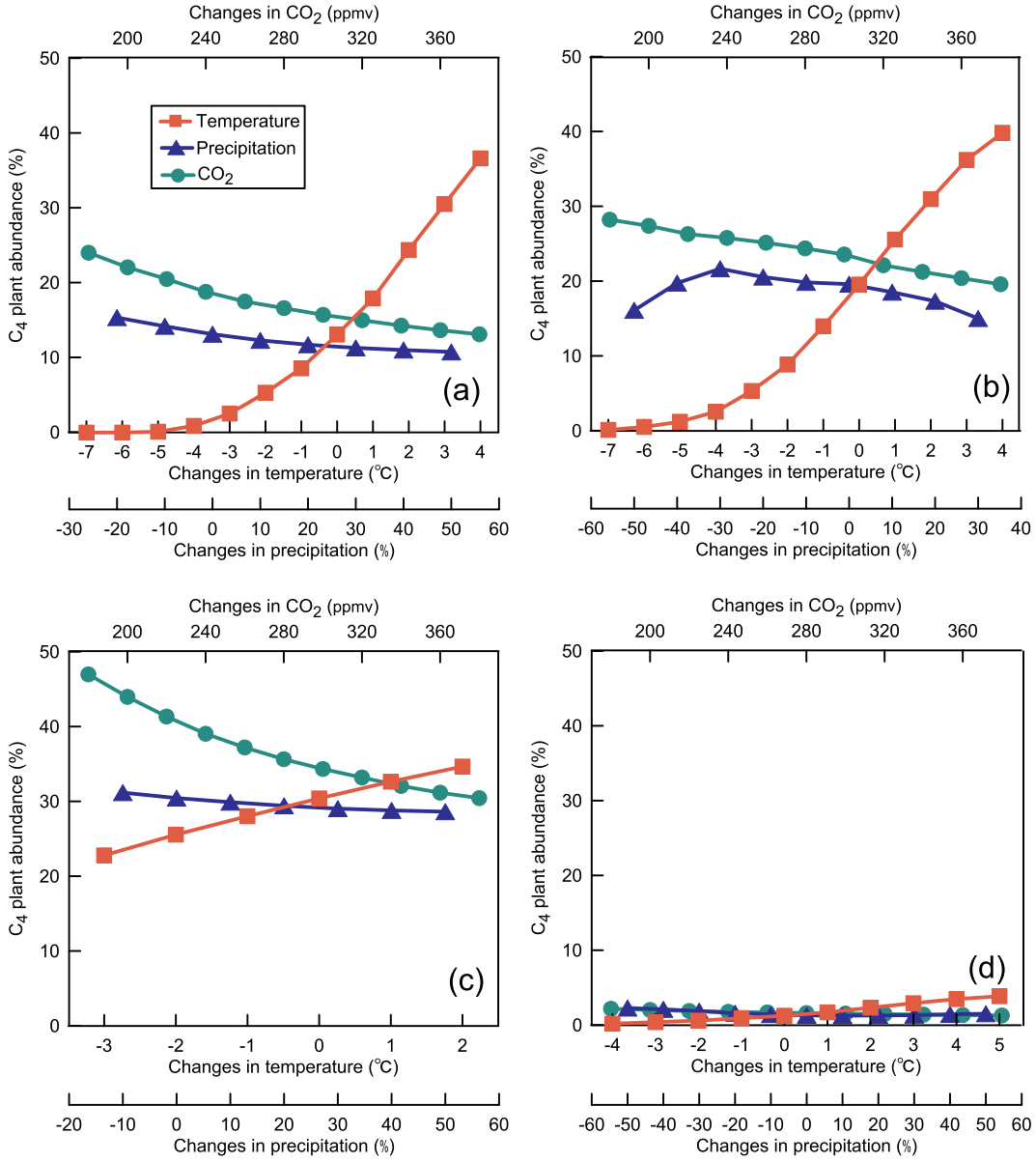

Fig. 5. Results of a sensitivity analysis of the response of the relative abundance of C_4 plants to changes in temperature, precipitation, and atmospheric CO_2 concentration.
a: Northeast China, b: CLP, c: South China, d: Tibetan Plateau. Red squares, blue triangles and green cycles represent temperature, precipitation and atmospheric CO_2 concentration. (For interpretation of the references to color in this figure legend, the reader is referred to the web version of this article.)

atmospheric pCO_2, suggesting that the changes in C_4 abundance on the CLP may were not driven primarily by precipitation or CO_2 levels.

Changes in C_4 abundance on the CLP are in-phase with temperature variations (Fig. 7a, c), with the maximum abundance C_4 coinciding with the temperature maximum during 10–6 kyr BP. Sensitivity analysis also revealed that C_4 abundance increased significantly with increasing temperature (Fig. 5b). This evidence leads us to conclude that the expansion of C_4 plants since the LGM on the CLP was mainly a response to rising temperature.

In Northeast China, the relationship of changing C_4 abundance to climatic records and atmospheric pCO_2 is consistent with that on the CLP (Fig. 7a, b), indicating that C_4 plants responded similarly to changes in climate and atmospheric CO_2 concentration in these two mid-latitude regions. Therefore, the expansion of C_4 plants in Northeast China during the Holocene was also caused primarily by rising temperature.

In South China, the sensitivity analysis indicates that C_4 abundance is positively correlated with temperature (Fig. 5c). If temperature was the main cause of changes in C_4 abundance, the warmer Holocene would have been expected to have exhibited a greater abundance of C_4 plants than the preceding colder glacial period. However, the occurrence of the opposite trend (Fig. 7a, d) suggests that other factors, rather than temperature, determined changes in C_4 abundance in the region.

Comparison of C_4 abundance in South China to the records of atmospheric pCO_2 and precipitation (or moisture level) shows that a higher abundance of C_4 plants occurred during the glacial period when atmospheric pCO_2 was lower and the climate was arid, while the opposite occurred during the Holocene (Fig. 7a, d). Sensitivity analysis also revealed that C_4 plants are better adapted to low CO_2 and

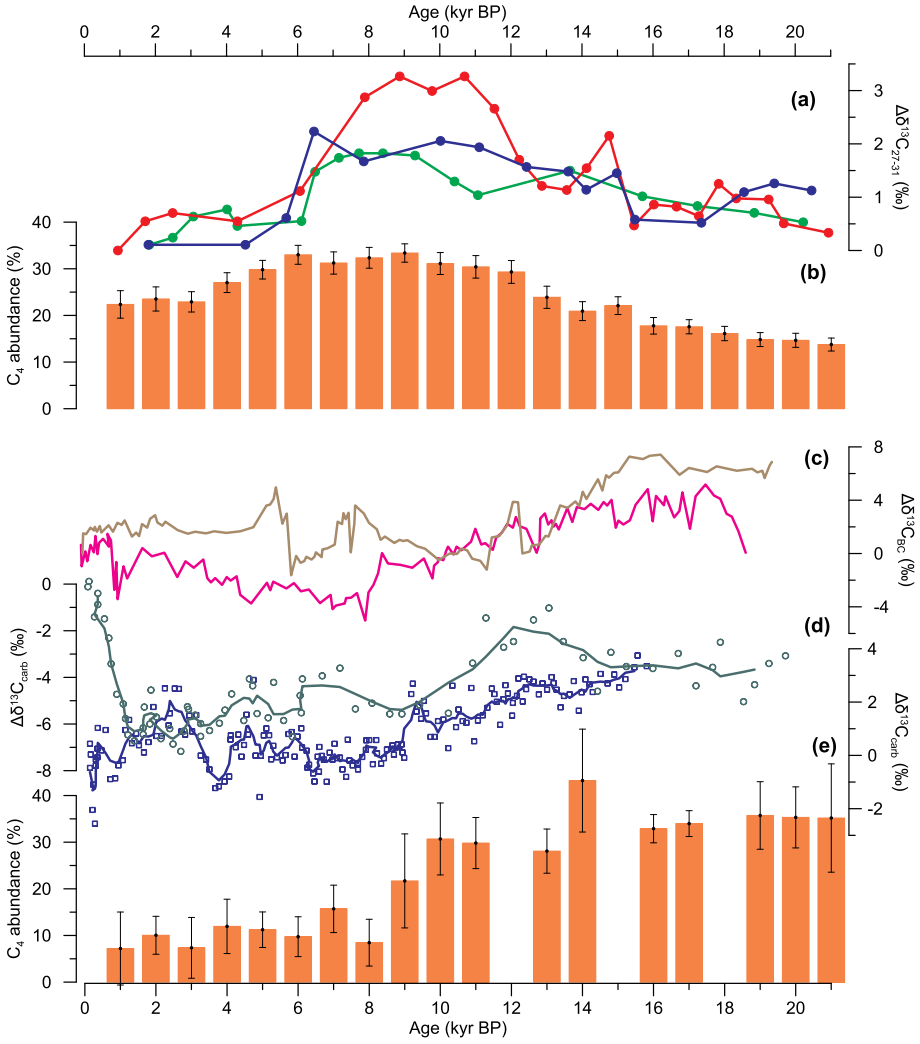

Fig. 6. Comparison of changes in C_4 plant abundance in South China and the CLP since the LGM with various published records
a: Weighted mean $\delta^{13}C_{27-31}$ of long-chain n-alkanes from Xifeng (green line) (Liu et al., 2005), Luochuan (red line) (Zhang et al., 2003) and Xunyi (blue line) (Zhang et al., 2003). b: Evolution of C_4 abundance on the CLP. c: Carbon isotopic composition of black carbon ($\delta^{13}C_{BC}$) at Lake TCQH (red line) (Zhang et al., 2015) and Lake Erhai (brown line) (Zhang et al., 2017). d: Carbonate $\delta^{13}C$ record ($\delta^{13}C_{carb}$) for Xiangshuiyan Cave (green circles are the measured values, and the green line is a five-point running mean) (Qin et al., 2000) and Dongge Cave (blue squares are the measured values, and the blue line is a five-point running mean) (Zhang et al., 2004). e: Evolution of C_4 abundance in South China. (For interpretation of the references to color in this figure legend, the reader is referred to the web version of this article.)

precipitation conditions than C_3 plants (Fig. 5c), and that temperature did not have a major influence on changes in C_4 plant abundance. Therefore, we suggest that the decrease in C_4 plant abundance in low-latitude South China was a response to the combined effect of increasing atmospheric pCO_2 and precipitation, especially the former.

On the Tibetan Plateau, sensitivity analysis revealed that the relative abundance of C_4 plants was insensitive to changes in temperature, precipitation or atmospheric pCO_2 (Fig. 5d). This is corroborated by the fact that reconstructed C_4 plant abundance in the region was remarkably constant since the LGM (Fig. 7e), because the lower growing season temperature during the past 21 kyr may have inhibited C_4 plant growth in this high-elevation region.

Our results highlight important regional differences in the dominant factors controlling the relative abundances of C_3 and C_4 plants in China since the LGM, which have also been pointed out in recent studies in East Africa (Urban et al., 2015) and southeastern Australia (Nelson et al., 2016). C_4 plant abundance in mid-latitude China was primarily controlled by temperature, as was also concluded for the mid-latitude North American Great Plains (e.g., Muhs et al., 1999; Johnson and Willey, 2000). In contrast, in low-latitude China, C_4 abundance was controlled by the combined effects of atmospheric pCO_2 and precipitation. This result is partly consistent with previous studies which suggest that either atmospheric pCO_2 (Street-Perrott et al., 1997; Huang et al., 1999; Damsté et al., 2011; Bragg et al., 2013) or precipitation (Huang et al., 2006; Castañeda et al., 2007; Contreras-Rosales et al., 2014) was the single most important factor determining changes in C_4 plants in low-latitude regions such as East Africa, South Asia and Mesoamerica. On the high elevation Tibetan Plateau, the low growing season temperature has resulted in the scarcity of C_4 plants.

5. Summary

We combined 33 $\delta^{13}C$ records of SOM from paleosol sequences and 16 $\delta^{13}C$ records of individual n-alkanes from lake sediments from across China, and reconstructed the spatiotemporal pattern of C_4 plant abundance since the LGM. The results show that South China had the highest C_4 abundance at the LGM, and that the CLP in North China had the highest abundance during the early to mid-Holocene. In North China, C_4 abundance increased since the LGM, reached a maximum during the early to mid-Holocene, and decreased thereafter. In contrast, in South China, C_4 abundance generally decreased during the Holocene. The high-elevation Tibetan Plateau experienced no significant change in the proportion of C_4 plants during the Holocene. Combined with a sensitivity analysis, our results reveal that C_4 plant expansion in mid-latitude China since the LGM was caused by rising temperatures, while the decrease in C_4 plants in low-latitude China was a response to increased atmospheric pCO_2 level and precipitation. On the Tibetan Plateau, the lower growing season temperature inhibited the growth of C_4 plants.

Supplementary data to this article can be found online at https://doi.org/10.1016/j.palaeo.2018.12.021.

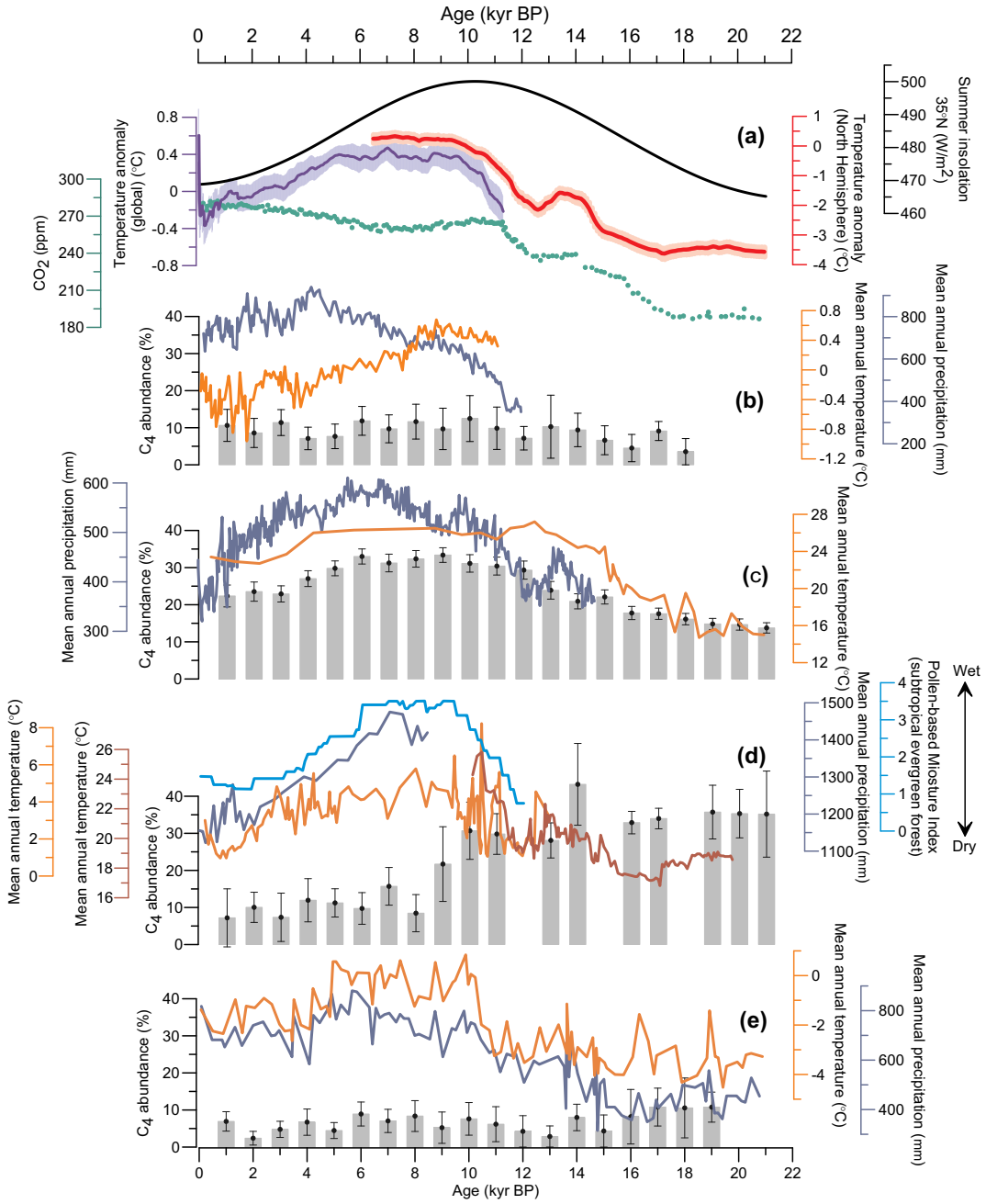

Fig. 7. Comparison of the relative abundance of C_4 plants in China with various climate proxies since the LGM.
a: Global mean temperature (Marcott et al., 2013) (purple line, temperature are given as anomalies from 1961–1990 CE mean), Northern Hemisphere temperature (Shakun et al., 2012) (red line, temperature are given as anomalies from 11.5–6.5 kyr mean), summer insolation at 35°N (Berger and Loutre, 1991) (black line) and atmospheric CO_2 concentration (Lüthi et al., 2008) (green dots). b: Evolution of the relative abundance of C_4 plants in Northeast China (grey bars), pollen-based MAP reconstruction from Sihailongwan Maar Lake in the Changbai Mountains region (Stebich et al., 2015) (blue line), and a pollen-based MAT reconstruction from Hulun Lake in northeastern Inner Mongolia (Wen et al., 2010) (orange line). c: Evolution of the relative abundance of C_4 plants on the CLP (grey bars), pollen-based MAP from Gonghai Lake on the northwestern margin of the CLP (Chen et al., 2015) (blue line) and a GDGTs-based reconstructed MAT record at Mangshan on the southeastern margin of the CLP (Peterse et al., 2011) (orange line). d: Evolution of the relative abundance of C_4 plants in South China (grey bar), pollen-based MAP reconstruction from Xingyun Lake in central Yunnan Province (Chen et al., 2014) (blue line), synthesized moisture index derived from pollen records from the subtropical evergreen forest region of South China (Zhao et al., 2009) (light blue line), fatty alcohol-based MAT record from Dajiuhu peat deposit in the Shennongjia Mountains (Huang et al., 2013) (orange line) and GDGTs-based MAT reconstruction from Huguangyan Maar Lake in the Leizhou Peninsula (red line) (Chu et al., 2017). e: Evolution of the relative abundance of C_4 plants on the Tibetan Plateau (grey bars) and pollen-based reconstruction of MAP (blue line) and MAT (orange line) from Lake Ximencuo in the Nianbaoyeze Mountains on the northeastern Tibetan Plateau (Herzschuh et al., 2014). The error bars represent the standard error of the mean. (For interpretation of the references to color in this figure legend, the reader is referred to the web version of this article.)

Acknowledgments

This research was funded by the National Basic Research Program of China (Grant no. 2016YFA0600504), the National Natural Science Foundation of China (Grant nos. 41572165, 41430531, 41690114, and 41125011), and the Bairen Programs of the Chinese Academy of Sciences.

References

Balesdent, J., Mariotti, A., 1996. Measurement of soil organic matter turnover using ^{13}C natural abundance. In: Boutton, T.W., Yamasaki, S.I. (Eds.), Mass Spectrometry of Soils. Marcel Dekker, New York, pp. 83–111.

Bartlein, P.J., Harrison, S.P., Brewer, S., Connor, S., Davis, B.A.S., Gajewski, K., Guiot, J., Harrison-Prentice, T.I., Henderson, A., Peyron, O., Prentice, I.C., Scholze, M., Seppä, H., Shuman, B., Sugita, S., Thompson, R.S., Viau, A.E., Williams, J., Wu, H.B., 2011. Pollen-based continental climate reconstructions at 6 and 21 ka: a global synthesis. Clim. Dyn. 37, 775–802.

Bender, M.M., 1971. Variations in the $^{13}C/^{12}C$ ratios of plants in relation to the path-way of photosynthetic carbon dioxide fixation. Phytochemistry 10, 1239–1245.

Berger, A., Loutre, M.F., 1991. Insolation values for the climate of the last 10 million years. Quat. Sci. Rev. 10, 297–317.

Berke, M.A., Johnson, T.C., Werne, J.P., Grice, K., Schouten, S., Damsté, J.S.S., 2012. Molecular records of climate variability and vegetation response since the Late Pleistocene in the Lake Victoria basin, East Africa. Quat. Sci. Rev. 55, 59–74.

Bragg, F.J., Prentice, I.C., Harrison, S.P., Eglinton, G., Foster, P.N., Rommerskirchen, F., Rullkötter, J., 2013. Stable isotope and modelling evidence for CO_2 as a driver of glacial-interglacial vegetation shifts in southern Africa. Biogeosciences 10, 2001–2010.

Brugnoli, E., Farquhar, G.D., 2000. Photosynthetic fractionation of carbon isotopes. In: Photosynthesis. Kluwer Academic Publishers, Netherlands, pp. 399–434.

Castañeda, I.S., Werne, J.P., Johnson, T.C., 2007. Wet and arid phases in the southeast African tropics since the Last Glacial Maximum. Geology 35, 823–826.

Cerling, T.E., Quade, J., Wang, Y., Bowman, J.R., 1989. Carbon isotopes in soils and palaeosols as ecology and palaoecology indicators. Nature 341, 138–139.

Chen, L.X., Zhu, Q.G., Luo, H.B., He, J.H., Dong, M., Feng, Z.Q., 1991. Monsoons over East Asia. Meteorological Press, Beijing (in Chinese).

Chen, F.H., Chen, X.M., Chen, J.H., Zhou, A.F., Wu, D., Tang, L.Y., Zhang, X.J., Huang, X.Z., Yu, J.Q., 2014. Holocene vegetation history, precipitation changes and Indian Summer Monsoon evolution documented from sediments of Xingyun Lake, southwest China. J. Quat. Sci. 29, 661–674.

Chen, F.H., Xu, Q.H., Chen, J.H., Birks, H.J.B., Liu, J.B., Zhang, S.R., Jin, L.Y., An, C.B., Telford, R.J., Cao, X.Y., Wang, Z.L., Zhang, X.J., Selvaraj, K., Lu, H.Y., Li, Y.C., Zheng, Z., Wang, H.P., Zhou, A.F., Dong, G.H., Zhang, J.W., Huang, X.Z., Bloemendal, J., Rao, Z.G., 2015. East Asian summer monsoon precipitation variability since the last deglaciation. Sci. Rep. 5, 1–11.

Chen, J.H., Rao, Z.G., Liu, J.B., Huang, W., Feng, S., Dong, G.H., Hu, Y., Xu, Q.H., Chen, F.H., 2016. On the timing of the East Asian summer monsoon maximum during the Holocene—does the speleothem oxygen isotope record reflect monsoon rainfall variability? Sci. China Earth Sci. 59, 2328–2338.

Chu, G.Q., Sun, Q., Zhu, Q.Z., Shan, Y.B., Shang, W.Y., Ling, Y., Su, Y.L., Xie, M.M., Wang, X.S., Liu, J., 2017. The role of the Asian winter monsoon in the rapid propagation of abrupt climate changes during the last deglaciation. Quat. Sci. Rev. 177, 120–129.

Clark, J.S., Grimm, E.C., Lynch, J., Mueller, P.G., 2001. Effects of Holocene climate change on the C_4 grassland/woodland boundary in the Northern Plains, USA. Ecology 82, 620–636.

Collatz, G.J., Berry, J.A., Clark, J.S., 1998. Effects of climate and atmospheric CO_2 partial pressure on the global distribution of C_4 grasses: present, past, and future. Oecologia 114, 441–454.

Collister, J.W., Rieley, G., Stern, B., Eglinton, G., Fry, B., 1994. Compound-specific $\delta^{13}C$ analyses of leaf lipids from plants with differing carbon dioxide metabolisms. Org. Geochem. 21, 619–627.

Contreras-Rosales, L.A., Jennerjahn, T., Tharammal, T., Meyer, V., Lückge, A., Paul, A., Schefuß, E., 2014. Evolution of the Indian Summer Monsoon and terrestrial vegetation in the Bengal region during the past 18 ka. Quat. Sci. Rev. 102, 133–148.

Damsté, J.S.S., Verschuren, D., Ossebaar, J., Blokker, J., Van Houten, R., Van der Meer, M.T., Plessen, B., Schouten, S., 2011. A 25,000-year record of climate-induced changes in lowland vegetation of eastern equatorial Africa revealed by the stable carbon-isotopic composition of fossil plant leaf waxes. Earth Planet. Sci. Lett. 302, 236–246.

Diefendorf, A.F., Freeman, K.H., Wing, S.L., Currano, E.D., Mueller, K.E., 2015. Paleogene plants fractionated carbon isotopes similar to modern plants. Earth Planet. Sci. Lett. 429, 33–44.

Dorale, J.A., González, L.A., Reagan, M.K., Pickett, D.A., Murrell, M.T., Baker, R.G., 1992. A high-resolution record of Holocene climate change in speleothem calcite from Cold Water Cave, northeast Iowa. Science 258, 1626–1630.

Dorale, J.A., Edwards, R.L., Ito, E., González, L.A., 1998. Climate and vegetation history of the midcontinent from 75 to 25 ka: a speleothem record from Crevice Cave, Missouri, USA. Science 282, 1871–1874.

Dubois, N., Oppo, D.W., Galy, V.V., Mohtadi, M., Kaars, S.V.D., Tierney, J.E., Rosenthal, Y., Eglinton, T.I., Lückge, A., Linsley, B.K., 2014. Indonesian vegetation response to changes in rainfall seasonality over the past 25,000 years. Nat. Geosci. 7, 513–517.

Eglinton, G., Hamilton, R.J., 1967. Leaf epicuticular waxes. Science 156, 1322–1335.

Ehleringer, J.R., Cerling, T.E., Helliker, B.R., 1997. C_4 photosynthesis, atmospheric CO_2, and climate. Oecologia 112, 285–299.

Farquhar, G.D., 1983. On the nature of carbon isotope discrimination in C_4 species. Aust. J. Plant Physiol. 10, 205–226.

Farquhar, G.D., Ehleringer, J.R., Hubick, K.T., 1989. Carbon isotope discrimination and photosynthesis. Annu. Rev. Plant Biol. 40, 503–537.

Food and Agriculture Organization (FAO), 1995. Digital Soil Map of the World and Derived Soil Properties. Food and Agriculture Organization, Rome.

Freyer, H.D., Belacy, N., 1983. $^{13}C/^{12}C$ records in northern hemispheric trees during the past 500 years-anthropogenic impact and climatic superpositions. J. Geophys. Res. Oceans 88, 6844–6852.

Galy, V., François, L., France-Lanord, C., Faure, P., Kudrass, H., Palhol, F., Singh, S.K., 2008. C_4 plants decline in the Himalayan basin since the Last Glacial Maximum. Quat. Sci. Rev. 27, 1396–1409.

Gu, Z.Y., Liu, Q., Xu, B., Han, J.M., Yang, S.L., Ding, Z.L., Liu, T.S., 2003. Climate as the dominant control on C_3 and C_4 plant abundance in the Loess Plateau: organic carbon isotope evidence from the last glacial-interglacial loess-soil sequences. Chin. Sci. Bull. 48, 1271–1276.

Guiot, J., Cheddadi, R., Prentice, I.C., Jolly, D., 1996. A method of biome and land surface mapping from pollen data: application to Europe 6000 years ago. Palaeoclimates: Data Model 1, 311–324.

Hatté, C., Guiot, J., 2005. Palaeoprecipitation reconstruction by inverse modelling using the isotopic signal of loess organic matter: application to the Nußloch loess sequence (Rhine Valley, Germany). Clim. Dyn. 25, 315–327.

Heller, F., Liu, T.S., 1984. Magnetism of Chinese loess deposits. Geophys. J. Int. 77, 125–141.

Herzschuh, U., Borkowski, J., Schewe, J., Mischke, S., Tian, F., 2014. Moisture-advection feedback supports strong early-to-mid Holocene monsoon climate on the eastern Tibetan Plateau as inferred from a pollen-based reconstruction. Palaeogeogr. Palaeoclimatol. Palaeoecol. 402, 44–54.

Hou, X., 2001. Vegetation Atlas of China. Science Press, Beijing (in Chinese).

Huang, Y., Street-Perrott, F.A., Perrott, R.A., Metzger, P., Eglinton, G., 1999. Glacial-interglacial environmental changes inferred from molecular and compound-specific $\delta^{13}C$ analyses of sediments from Sacred Lake, Mt. Kenya. Geochim. Cosmochim. Acta 63, 1383–1404.

Huang, Y., Street-Perrott, F.A., Metcalfe, S.E., Brenner, M., Moreland, M., Freeman, K.H., 2001. Climate change as the dominant control on glacial-interglacial variations in C_3 and C_4 plant abundance. Science 293, 1647–1651.

Huang, Y.S., Shuman, B., Wang, Y., Iii, T.W., Grimm Jr., E.C., G.L.J., 2006. Climatic and environmental controls on the variation of C_3 and C_4 plant abundances in central Florida for the past 62,000 years. Palaeogeogr. Palaeoclimatol. Palaeoecol. 237, 428–435.

Huang, X.Y., Meyers, P.A., Jia, C.L., Zheng, M., Xue, J.T., Wang, X., Xie, S.C., 2013. Paleotemperature variability in central China during the last 13 ka recorded by a novel microbial lipid proxy in the Dajiuhu peat deposit. The Holocene 23, 1123–1129.

Jiang, D., Lang, X., Tian, Z., Guo, D., 2011. Last glacial maximum climate over China from pmip simulations. Palaeogeogr. Palaeoclimatol. Palaeoecol. 309, 347–357.

Johnson, W.C., Willey, K.L., 2000. Isotopic and rock magnetic expression of environmental change at the Pleistocene-Holocene transition in the central Great Plains. Quat. Int. 67, 89–106.

Kang, S.G., Wang, X.L., Lu, Y.C., 2013. Quartz OSL chronology and dust accumulation rate changes since the Last Glacial at Weinan on the southeastern Chinese Loess Plateau. Boreas 42, 815–829.

Kaplan, J.O., Bigelow, N.H., Prentice, I.C., Harrison, S.P., Bartlein, P.J., Christensen, T.R., Cramer, W., Matveyeva, N.V., McGuire, A.D., Murray, D.F., Razzhivin, V.Y., Smith, B., Walker, D.A., Anderson, P.M., Andreev, A.A., Brubaker, L.B., Edwards, M.E., Lozhkin, A.V., 2003. Climate change and Arctic ecosystems: 2. Modeling, paleodata-model comparisons, and future projections. J. Geophys. Res. 108, 1–12.

Kohn, M., 2016. Carbon isotope discrimination in C_3 land plants is independent of nature variation in pCO2. Geochem. Perspect. Lett. 2, 35–43.

Körner, C., 2007. The use of 'altitude' in ecological research. Trends Ecol. Evol. 22, 569–574.

Körner, C., Farquhar, G.D., Roksandic, Z., 1988. A global survey of carbon isotope discrimination in plants from high altitude. Oecologia 74, 623–632.

Kuang, H.Z., Zhou, H.D., Hu, J.F., Yang, X.Q., Peng, P.A., Yang, H., 2013. Variation of n-alkanes and compound-specific carbon isotope in sediment from Huguangyan maar lake during the Last Glacial Maximum and Holocene optimum: implications for paleovegetation. Quat. Sci. 33, 1222–1233 (in Chinese).

Kukla, G., An, Z.S., 1989. Loess stratigraphy in central China. Palaeogeogr. Palaeoclimatol. Palaeoecol. 72, 203–225.

Liu, T.S., 1985. Loess and the Environment. Science Press, Beijing (in Chinese).

Liu, K.B., 1988. Quaternary history of the temperate forests of China. Quat. Sci. Rev. 7 (1), 1–20.

Liu, W.G., Huang, Y.S., An, Z.S., Clemens, S.C., Li, L., Prell, W.L., Ning, Y.F., 2005. Summer monsoon intensity controls C_4/C_3 plant abundance during the last 35 ka in the Chinese Loess Plateau: carbon isotope evidence from bulk organic matter and individual leaf waxes. Palaeogeogr. Palaeoclimatol. Palaeoecol. 220, 243–254.

Lloyd, J., Farquhar, G.D., 1994. $\delta^{13}C$ discrimination during CO_2 assimilation by the terrestrial biosphere. Oecologia 99, 201–215.

Luo, K.F., 1954. Zoning issue of Physical Geography of China. Chin. Sci. Bull. 68-71 (in Chinese).

Lüthi, D., Le Floch, M., Bereiter, B., Blunier, T., Barnola, J.M., Siegenthaler, U., Raynaud, D., Jouzel, J., Fischer, H., Kawamura, K., Stocker, T.F., 2008. High-resolution carbon dioxide concentration record 650,000–800,000 years before present. Nature 453, 379–382.

Marcott, S.A., Shakun, J.D., Clark, P.U., Mix, A.C., 2013. A reconstruction of regional and global temperature for the past 11,300 years. Science 339, 1198–1201.

Masson-Delmotte, V., Schulz, M., Abe-Ouchi, A., Beer, J., Ganopolski, A., González Rouco, J.F., Jansen, E., Lambeck, K., Luterbacher, J., Naish, T., Osborn, T., Otto-Bliesner, B., Quinn, T., Ramesh, R., Rojas, M., Shao, X., Timmermann, A., 2013. Information from paleoclimate archives. In: Stocker, T.F., Qin, D., Plattner, G.-K., Tignor, M., Allen, S.K., Boschung, J., Nauels, A., Xia, Y., Bex, V., Midgley, P.M. (Eds.), Climate Change 2013: The Physical Science Basis. Cambridge University Press, Cambridge, United Kingdom and New York, pp. 383–464.

Mauna Loa Observatory, 2000. ftp://aftp.cmdl.noaa.gov/data/trace_gases/co2c13/flask/surface/co2c13_mlo_surface-flask_1_sil_month.txt.

Melillo, J.M., Aber, J.D., Linkins, A.E., Ricca, A., Fry, B., Nadelhoffer, K.J., 1989. Carbon and nitrogen dynamics along the decay continuum: plant litter to soil organic matter. Plant Soil 115, 189–198.

Muhs, D.R., Aleinikoff, J.N., Stafford, T.W., Kihl, R., Been, J., Mahan, S.A., Cowherd, S., 1999. Late Quaternary loess in northeastern Colorado: part I-Age and paleoclimatic significance. Geol. Soc. Am. Bull. 111, 1861–1875.

Nelson, D.M., Urban, M.A., Kershaw, A.P., Hu, F.S., 2016. Late-Quaternary variation in C_3 and C_4 grass abundance in southeastern Australia as inferred from $\delta^{13}C$ analysis:

assessing the roles of climate, pCO_2, and fire. Quat. Sci. Rev. 139, 67–76.
Norström, E., Neumann, F.H., Scott, L., Smittenberg, R.H., Holmstrand, H., Lundqvist, S., Snowball, I., Sundqvist, H.S., Risberg, J., Bamford, M., 2014. Late Quaternary vegetation dynamics and hydro-climate in the Drakensberg, South Africa. Quat. Sci. Rev. 105, 48–65.
Peterse, F., Prins, M.A., Beets, C.J., Troelstra, S.R., Zheng, H.B., Gu, Z.Y., Schoutena, S., Damsté, J.S.S., 2011. Decoupled warming and monsoon precipitation in East Asia over the last deglaciation. Earth Planet. Sci. Lett. 301, 256–264.
Qin, J.M., Yuan, D.X., Lin, Y.S., Zhang, M.L., Li, B., 2000. Isotopic records of stalagmites from Guilin since 44 ka BP and their environmental interpretation. Acta Geosci. Sin. 21, 407–416.
Rao, Z., Zhu, Z., Zhang, J., 2007. Different climatic controls of soil $\delta^{13}C$ org in three mid-latitude regions of the Northern Hemisphere since the Last Glacial period. Chin. Sci. Bull. 52 (2), 259.
Rao, Z., Jia, G., Zhu, Z., Wu, Y., Zhang, J., 2008. Comparison of the carbon isotope composition of total organic carbon and long-chain n-alkanes from surface soils in eastern China and their significance. Chin. Sci. Bull. 53, 3921–3927.
Rao, Z.G., Chen, F.H., Zhang, X., Xu, Y.B., Xue, Q., Zhang, P.Y., 2012. Spatial and temporal variations of C_3/C_4 relative abundance in global terrestrial ecosystem since the Last Glacial and its possible driving mechanisms. Chin. Sci. Bull. 57, 4024–4035.
Ratnayake, N.P., Suzuki, N., Okada, M., Takagi, M., 2006. The variations of stable carbon isotope ratio of land plant-derived n-alkanes in deep-sea sediments from the Bering Sea and the North Pacific Ocean during the last 250,000 years. Chem. Geol. 228, 197–208.
Raven, P.H., Evert, R.F., Eichhorn, S.E., 1999. Biology of Plants. Freeman and Company Worth Publishers, New York, pp. 126–153.
Reimer, P.J., Bard, E., Bayliss, A., Beck, J.W., Blackwell, P.G., Ramsey, C.B., Buck, C.E., Cheng, H., Edwards, R.L., Friedrich, M., Grootes, P.M., Guilderson, T.P., Haflidason, H., Hajdas, I., Hatté, C., Heaton, T.J., Hoffmann, D.L., Hogg, A.G., Hughen, K.A., Kaiser, K.F., Kromer, B., Manning, S.W., Niu, M., Reimer, R.W., Richards, D.A., Scott, E.M., Southon, J.R., Staff, R.A., Turney, C.S.M., van der Plicht, J., 2013. IntCal13 and Marine13 radiocarbon age calibration curves 0–50,000 years cal BP. Radiocarbon 55, 1869–1887.
Rieley, G., Collier, R.J., Jones, D.M., Eglinton, G., Eakin, P.A., Fallick, A.E., 1991. Sources of sedimentary lipids deduced from stable carbon-isotope analyses of individual compounds. Nature 352, 425.
Sage, R.F., 2001. Environmental and evolutionary preconditions for the origin and diversification of the C_4 photosynthetic syndrome. Plant Biol. 3, 202–203.
Sage, R.F., Wedin, D.A., Li, M., 1999. The biogeography of C_4 photosynthesis. In: Sage, R.F. (Ed.), C_4 Plant Biology. Academic Press, America, pp. 313–373.
Samal, A., Martin, O.C., 2013. Shining fresh light on the evolution of photosynthesis. elife 2, e1403.
Schmitt, J., Schneider, R., Elsig, J., Leuenberger, D., Lourantou, A., Chappellaz, J., Köhler, P., Joos, F., Stocker, T.F., Leuenberger, M., Fischer, H., 2012. Carbon isotope constraints on the deglacial CO_2 rise from ice cores. Science 336, 711–714.
Schubert, B.A., Jahren, A.H., 2012. The effect of atmospheric CO_2 concentration on carbon isotope fractionation in C_3 land plants. Geochim. Cosmochim. Acta 96, 29–43.
Shakun, J.D., Clark, P.U., He, F., Marcott, S.A., Mix, A.C., Liu, Z.Y., Otto-Bliesner, B., Schmittner, A., Bard, E., 2012. Global warming preceded by increasing carbon dioxide concentrations during the last deglaciation. Nature 484, 49–54.
Shi, Y.F., Kong, Z.Z., Wang, S.M., Tang, L.Y., Wang, F.B., Yao, T.D., Zhao, X.T., Zhang, P.Y., Shi, S.H., 1993. Mid-Holocene climates and environments in China. Glob. Planet. Chang. 7, 219–233.
Sponheimer, M., Lee-Thorp, J.A., 1999. Isotopic evidence for the diet of an early hominid, *Australopithecus africanus*. Science 283, 368–370.
Stebich, M., Rehfeld, K., Schlütz, F., Tarasov, P.E., Liu, J., Mingram, J., 2015. Holocene vegetation and climate dynamics of ne China based on the pollen record from Sihailongwan Maar lake. Quat. Sci. Rev. 124, 275–289.
Stewart, G.R., Turnbull, M.H., Schmidt, S., Reskine, P.D., 1995. ^{13}C natural abundance in plant communities along a rainfall gradient: a biological integrator of water availability. Aust. J. Plant Physiol. 22, 51–55.
Street-Perrott, F.A., Huang, Y.S., Perrott, R.A., Eglinton, G., Barker, P., Khelifa, L.B., Harkness, D.D., Olago, D.O., 1997. Impact of lower atmospheric carbon dioxide on tropical mountain ecosystems. Science 278, 1422–1426.
Tipple, B.J., Pagani, M., 2010. A 35 Myr North American leaf-wax compound-specific carbon and hydrogen isotope record: implications for C_4 grasslands and hydrologic cycle dynamics. Earth Planet. Sci. Lett. 299, 250–262.
Urban, M.A., Nelson, D.M., Street-Perrott, F.A., Verschuren, D., Hu, F.S., 2015. A late-Quaternary perspective on atmospheric pCO_2, climate, and fire as drivers of C_4-grass abundance. Ecology 96, 642–653.
Van de Water, P.K., Leavitt, S.W., Betancourt, J.L., 2002. Leaf $\delta^{13}C$ variability with elevation, slope aspect, and precipitation in the southwest United States. Oecologia 132, 332–343.
Vidic, N.J., Montañez, I.P., 2004. Climatically driven glacial-interglacial variations in C_3 and C_4 plant proportions on the Chinese Loess Plateau. Geology 32, 337–340.
Voelker, S.L., Brooks, J.R., Meinzer, F.C., Anderson, R., Bader, M.K., Battipaglia, G., Becklin, K.M., Beerling, D., Bert, D., Betancourt, J.L., Dawson, T.E., Domec, J.-C., Guyette, R.P., Körner, C., Leavitt, S.W., Linder, S., Marshall, J.D., Mildner, M., Ogée, J., Panyushkina, I., Plumpton, H.J., Pregitzer, K.S., Saurer, M., Smith, A.R., Siegwolf, R.T.W., Stambaugh, M.C., Talhelm, A.F., Tardif, J.C., Van de Water, P.K., Ward, J.K., Wingate, L., 2016. A dynamic leaf gas-exchange strategy is conserved in woody plants under changing ambient CO_2: evidence from carbon isotope discrimination in paleo and CO_2 enrichment studies. Glob. Chang. Biol. 22, 889.
Wang, P., 2009. Global monsoon in a geological perspective. Chin. Sci. Bull. 54, 1113–1136.
Wang, R.Z., Ma, L.N., 2016. Climate-driven C_4 plant distributions in China: divergence in C_4 taxa. Sci. Rep. 6, 27977.
Wang, G., Feng, X., Han, J., Zhou, L., Tan, W., Su, F., 2008. Paleovegetation reconstruction using? ^{13}C of Soil Organic Matter. Biogeosci. Discuss. 5, 1795–1823.
Wang, S., Lu, H., Han, J., Chu, G., Liu, J., Negendank, J.F., 2012. Palaeovegetation and palaeoclimate in low-latitude southern China during the last Glacial Maximum. Quat. Int. 248, 79–85.
Wang, Y.V., Larsen, T., Leduc, G., Andersen, N., Blanz, T., Schneider, R.R., 2013. What does leaf wax δD from a mixed C_3/C_4 vegetation region tell us? Geochim. Cosmochim. Acta 111, 128–139.
Wang, G., Wang, Y.L., Meng, P., Wang, Z.X., Sun, Z.P., Yang, H., Gong, J.C., Zhang, H., Wu, Y.Q., Wang, Y.X., 2015. Chemical and compound-specific carbon isotope characteristics of n-alkanes in the Qingshi lacustrine sediments, Wudalianchi, Northeast China, and their paleovegetation significances. Quat. Sci. 35, 890–900 (in Chinese).
Wen, R.L., Xiao, J.L., Chang, Z.G., Zhai, D.Y., Xu, Q.H., Li, Y.C., Itoh, S., 2010. Holocene precipitation and temperature variations in the East Asian monsoonal margin from pollen data from Hulun Lake in northeastern Inner Mongolia, China. Boreas 39, 262–272.
Wu, N.Q., Liu, T.S., Liu, X.P., Gu, Z.Y., 2002. Mollusk record of millennial climate variability in the Loess Plateau during the Last Glacial Maximum. Boreas 31, 20–27.
Wu, H.B., Guo, Z.T., Guiot, J., Hatté, C., Peng, C., Yu, Y.Y., Ge, J.Y., Li, Q., Sun, A.Z., Zhao, D., 2014. Elevation-induced climate change as a dominant factor causing the late Miocene C_4 plant expansion in the Himalayan foreland. Glob. Chang. Biol. 20, 1461–1472.
Wu, H.B., Li, Q., Yu, Y.Y., Jiang, W.Q., Lin, Y.T., Sun, A.Z., Luo, Y.L., 2017. Quantitative climate reconstruction in China during the mid-Holocene. Quat. Sci. 37, 982–998 (in Chinese).
Wu, H.B., Li, Q., Yu, Y.Y., Sun, A.Z., Lin, Y.T., Jiang, W.Q., Luo, Y.L., 2018. Quantitative Climate Reconstruction in China during the Last Glacial Maximum. (Submitted to Sci. China).
Xue, J., Zhong, W., Cao, J., 2014. Changes in C_3 and C_4 plant abundances reflect climate changes from 41,000 to 10,000 yr ago in northern Leizhou Peninsula, South China. Palaeogeogr. Palaeoclimatol. Palaeoecol. 396, 173–182.
Yamada, K., Ishiwatari, R., 1999. Carbon isotopic compositions of long-chain n-alkanes in the Japan Sea sediments: implications for paleoenvironmental changes over the past 85 kyr. Org. Geochem. 30, 367–377.
Yang, S.L., Ding, Z.L., Li, Y.Y., Wang, X., Jiang, W.Y., Huang, X.F., 2015. Warming-induced northwestward migration of the East Asian monsoon rain belt from the Last Glacial Maximum to the mid-Holocene. Proc. Natl. Acad. Sci. U. S. A. 112, 13178–13183.
Yao, Z., Wu, H., Liang, M., Shi, X., 2011. Spatial and temporal variations in C_3 and C_4 plant abundance over the Chinese Loess Plateau since the last glacial maximum. J. Arid Environ. 75, 881–889.
Yin, L.J., Li, M.R., 1997. A study on the geographic distribution and ecology of C_4 plants in China. I. C4 plant distribution in China and their relation with regional climatic condition. Acta Ecol. Sin. 17, 350–363 (in Chinese).
Zhang, Z.H., Zhao, M.X., Lu, H.Y., Faiia, A.M., 2003. Lower temperature as the main cause of C_4 plant declines during the glacial periods on the Chinese Loess Plateau. Earth Planet. Sci. Lett. 214, 467–481.
Zhang, M.L., Cheng, H., Lin, Y.S., Qin, J.M., Zhang, H.L., Tu, L.L., Wang, H., Feng, Y.M., 2004. High resolution paleoclimatic environment records from a stalagmite of Dongge Cave since 15000a in Libo, Guizhou Province, China. Geochimica 33, 65–74 (in Chinese).
Zhang, E., Sun, W., Zhao, C., Wang, Y., Xue, B., Shen, J., 2015. Linkages between climate, fire and vegetation in southwest China during the last 18.5 ka based on a sedimentary record of black carbon and its isotopic composition. Palaeogeogr. Palaeoclimatol. Palaeoecol. 435, 86–94.
Zhang, E.L., Sun, W.W., Liu, E.F., Ning, D.L., 2017. Vegetation change reconstructed by a stable isotope record of elemental carbon from Lake Erhai, southwest China since the last glacial maximum. Quat. Sci. 37, 1027–1036 (in Chinese).
Zhao, Y., Yu, Z., Chen, F., Zhang, J., Yang, B., 2009. Vegetation response to Holocene climate change in monsoon-influenced region of China. Earth Sci. Rev. 97, 242–256.
Zhou, Y., Fan, J., Zhang, W., Harris, W., Zhong, H., Hu, Z., Song, L., 2011. Factors influencing altitudinal patterns of C_3, plant foliar carbon isotope composition of grasslands on the Qinghai-Tibet Plateau, China. Alp. Bot. 121, 79–90.
Zhou, B., Zheng, H.B., Yang, W.G., Taylor, D., Lu, Y.H., Wei, G.J., Li, L., Wang, H., 2012. Climate and vegetation variations since the LGM recorded by biomarkers from a sediment core in the northern South China Sea. J. Quat. Sci. 27, 948–955.
Zhu, Y., Siegwolf, R.T., Durka, W., Körner, C., 2010. Phylogenetically balanced evidence for structural and carbon isotope responses in plants along elevational gradients. Oecologia 162, 853–863.